A Bidirectional Three-Phase Push–Pull Converter With Hybrid PPS-DAPWM Switching Method for High Power and Wide Voltage Range Applications

Tat-Thang Le, *Student Member, IEEE*, Hyeonju Jeong, and Sewan Choi, *Fellow, IEEE*

***Abstract*—High-power isolated bidirectional dc–dc converters with wide voltage range are attracting increasing attention in many applications. The bidirectional three-phase current-fed dc–dc converters are known to be suitable for wide voltage range applications compared to dual active bridge based converters, having advantages of reduced device current ratings and prevention of transformer saturation due to high impedance nature. However, when the duty cycle becomes lower than 0.33 or higher than 0.66, power transfer capability is limited, and the efficiency is significantly reduced due to increased circulating current, which has rarely been discussed so far. In this article, a hybrid dual-asymmetrical pulsewidth modulation (DAPWM) and pulsewidth modulation plus phase-shift (PPS) switching method is proposed for efficiency improvement of the bidirectional three-phase push–pull converter with very wide voltage range. A seamless mode change method between PPS and DAPWM is also proposed for minimizing the transient state. Further, through current waveform and power flow analysis, the leakage inductance along with transformer turn ratio are designed to minimize the root mean square (rms) current of devices, while having the capability of transferring the desired power and limiting the slew rate of transformer winding current under wide voltage range operation. Experimental results from a 22-kW prototype are provided to validate the proposed concept.**

***Index Terms*—Bidirectional dc–dc converter, circulating current, current-fed, dead-time effect, high power, wide voltage range.**

I. Introduction

RECENTLY, high-power isolated bidirectional dc–dc converters with the wide voltage range have aroused much interest in many applications such as energy storage systems, uninterruptible power supplies, electric vehicles, renewable energy systems, and dc microgrid systems. In high power applications, the three-phase dc–dc converter has several advantages over the single-phase dc–dc converter such as easy switch selection due to reduced current rating, reduction of input and output filters' volume due to increased effective switching frequency by a factor of three, and reduction in transformer volume due to better transformer utilization [1].

The three phase dual active bridge (DAB) converters have been widely used in solid state transformers where the main operating voltage range is not wide [1]–[8]. Due to the voltage-fed nature of both sides, the DAB suffers from possible transformer saturation and large circulating current, and loss of zero voltage switching (ZVS) at the light load when operated under the wide voltage range [1]. The voltage-fed types have simple structure but it has disadvantage of high ripple current in the low voltage side (LVS) [9]. In response to these concerns, bidirectional three-phase current-fed dc–dc converters with active clamp have been introduced in [10]–[22]. By utilizing the active clamp, the current-fed dc–dc converter not only clamps the surge voltage [24] but also has smaller circulating current under wide voltage range. The entire range ZVS of all switches can be achieved by proper design of the filter and the leakage inductances [12]. Also, the current-fed converter has smaller current ripple compared to the voltage-fed converter. Further, due to the high impedance nature of the current-fed converter, transformer saturation can be avoided [22]. There are two types of bidirectional three-phase current-fed converters with active clamp: half-bridge [12] and push–pull converters [13]. The three-phase current-fed half-bridge converter preserves the advantage of entire range ZVS, smaller circulating current, and ripple current. However, sophisticated balancing control using three current sensors is required to balance three filter inductor currents [12]. The three-phase current-fed push–pull converter using one filter inductor and one current sensor has been introduced in [13] where the effective frequency across the filter inductor is three times of the switching frequency, resulting in significantly reduced core volume and loss of the filter inductor.

In [12] and [13], the pulsewidth modulation plus phase-shift (PPS) and dual-asymmetrical pulsewidth modulation (DAPWM) switching methods were proposed for the

Manuscript received September 28, 2019; revised December 11, 2019; accepted January 2, 2020. Date of publication January 29, 2020; date of current version October 30, 2020. This work was supported in part by the National Research Foundation of Korea (NRF) grant funded by the Korea government (MSIT) (2017R1A2A2A05001054), and Human Resources Development of Korea Institute of Energy Technology Evaluation and Planning (KETEP) grant funded by the Korea Government Ministry of Trade, Industry & Energy (No. 20174030201840). *(Corresponding author: Sewan Choi.)*

The authors are with the Department of Electrical and Information Engineering, Seoul National University of Science and Technology, Seoul 139-743, South Korea (e-mail: lethang@seoultech.ac.kr; hyeonju0618@seoultech.ac.kr; schoi@seoultech.ac.kr).

Color versions of one or more of the figures in this article are available online at https://ieeexplore.ieee.org.

Digital Object Identifier 10.1109/TIE.2020.2969113

0278-0046 © 2020 IEEE. Personal use is permitted, but republication/redistribution requires IEEE permission.
See https://www.ieee.org/publications/rights/index.html for more information.

Authorized licensed use limited to: Seoul National Univ of Science & Tech (SNUT). Downloaded on November 06,2020 at 08:04:53 UTC from IEEE Xplore. Restrictions apply.

three-phase current-fed converter to regulate the transferred power while maintaining the clamp voltage the same with high voltage side (HVS) voltage referred to the LVS voltage so that the circulating current is reduced under the LVS voltage variation. However, most of the previous literatures on the current-fed dc–dc converters with active clamp [12]-–[13] deal with operation with the duty cycle (D) *only* between 0.33 and 0.66. So far, *wide* voltage range operation with the duty cycle smaller than 0.33 or larger than 0.66 has not been rarely implemented or analyzed in detail. The converter in [25] tried to increase D range with PPS switching method, however, in higher D range (D>0.66), the circulating current becomes larger. The analysis and experiment results just show the high circulating current when D is 0.725, and does not provide any solution, resulting in limitation of voltage range.

In general, in the high voltage and high power application, a large dead time is required for preventing the converter from shoot through during a switching interval [26]-–[29]. It will be shown in this article that DAPWM (PPS) with *large* dead time dramatically increases circulating current especially when the duty cycle gets smaller than 0.33 (larger than 0.66), and therefore limits the power transfer capability.

In this article, through comprehensive comparison between PPS and DAPWM including dead-time effect on circulating current, power transfer area, rms current, and power flow under whole duty range, a hybrid-switching method is newly proposed. The proposed switching method greatly reduced the circulating current loss in the low (<0.33) and high (>0.66) duty cycle range compared to only PPS and only DAPWM, respectively. Also, a seamless mode change method between PPS and DAPWM is proposed for minimizing the current and voltage transient under the mode change.

In order to be capable of transferring the desired power under wide voltage range ($D < 0.33$ or $D > 0.66$), the leakage inductance L_k should be decreased. However, this causes so called, "high slew rate of transformer winding current" [23], [24], resulting in high peak transformer winding current. This article designed the leakage inductance value along with transformer turn ratio so that the slew rate of transformer winding current is limited and the rms current is reduced while having the capability of transferring the desired power.

The proposed hybrid switching method and design method can be applied for general bidirectional three-phase current-fed (push–pull or half-bridge) converters with the active clamp, which have same problems under wide voltage range application in [12], [13], and [30].

A 22 kW bidirectional three-phase push–pull converter was built and tested to verify the validity of the proposed operation.

II. Analysis of Two Switching Methods for Bidirectional Three-Phase Push–Pull Converter

Fig. 1 shows the configuration of the bidirectional three-phase push–pull converter with the active clamp introduced in [13]. The PPS switching method is a technique combining pulsewidth modulation control technique and phase-shift control technique; duty cycles of top switches D_L and D_H of the primary and

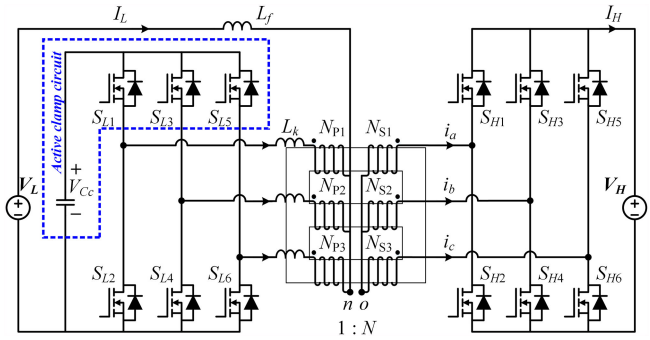

Fig. 1. Circuit diagram of the current-fed bidirectional three-phase push–pull converter.

secondary sides are the same and used for controlling the active clamp voltage; and the phase-shift, D_φ, is used for controlling the power. D_φ is defined as $\varphi/2\pi$, φ is phase-shift between sides in radian. The DAPWM switching method uses two independent duty cycles, D_L and ΔD; the active clamp voltage is controlled by LVS duty cycle D_L and power is controlled by ΔD $(= D_H - D_L)$ that is difference between D_H and D_L.

Switching patterns of two switching methods of DAPWM and PPS for each phase of the converter are given in Table I. There is 120° between phases. The control variables of DAPWM and PPS switching methods are D_L, ΔD and D_L, D_φ, respectively. The duty cycle D_L is used to control $V_{Cc} = V_H/N$ for minimizing the circulating current, where N is the transformer turn ratio. The power is regulated by ΔD and D_φ. The power flow direction of the converter is determined by the sign of ΔD and D_φ: the negative sign for the reverse mode from HVS to LVS, and the positive sign for the forward mode from LVS to HVS. Neglecting dead time T_d, the ratio of V_L and V_{Cc} is expressed as

$$\frac{V_L}{V_{Cc}} = D_L \tag{1}$$

However, in case of large dead time T_d, the ratio V_L/V_{Cc} depends on T_d. The effect of the dead time on the clamp voltage is detailed in the next sections.

A. Operation Principles According to Switching Methods and Duty Range

In case of wide voltage range, three operation ranges of D_L should be considered in both switching methods: low D_L range $(D_L < 0.33)$, medium D_L range $(0.33 < D_L < 0.66)$, and high D_L range $(D_L > 0.66)$. Fig. 2 shows the key waveforms in forward mode, for DAPWM and PPS switching methods. It is noted in this figure that there exist two notable intervals regarding the switching methods and duty range: power transfer interval and the circulating current interval, which exists in both reverse and forward modes.

In the medium D_L range, both PPS and DAPWM switching methods have no circulating current interval. It is seen from current I_H that the power is always being transferred to the load. The rms values of the transformer winding currents of

Authorized licensed use limited to: Seoul National Univ of Science & Tech (SNUT). Downloaded on November 06,2020 at 08:04:53 UTC from IEEE Xplore. Restrictions apply.

TABLE I
TWO SWITCHING METHODS FOR THE BIDIRECTIONAL THREE-PHASE PUSH–PULL CONVERTER

Switching methods	DAPWM	PPS
Switching patterns	D_LT_S, T_d, $(1\text{-}D_L)T_S$, S_{L1}, S_{L2}; D_HT_S, $(1\text{-}D_H)T_S$, S_{H1}, S_{H2}; ΔDT_S; $\Delta D=D_H-D_L$	D_LT_S, T_d, $(1\text{-}D_L)T_S$, S_{L1}, S_{L2}; D_HT_S, $(1\text{-}D_H)T_S$, S_{H1}, S_{H2}; $D_\varphi T_S$; $D_H=D_L$, $D_\varphi=\varphi/2\pi$
Control variables	D_L, ΔD	$D_L(=D_H)$, D_φ

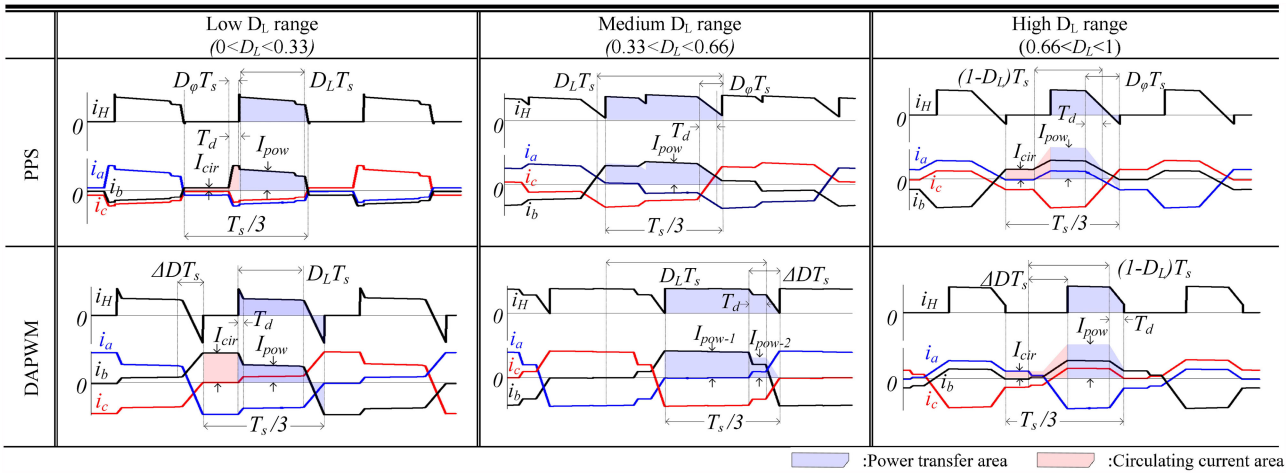

Fig. 2. Key waveforms of secondary transformer current and load current of PPS and DAPWM with different D_L in forward mode.

TABLE II
COMPARISON OF PPS AND DAPWM SWITCHING METHODS CONSIDERING WIDE LVS RANGE AND DEAD TIME

Operation range of Duty cycle	DAPWM		PPS	
	Circulating current	Power transfer area	Circulating current	Power transfer area
Low D_L range D_L<0.33	Larger (Always appear the circulating current)	Smaller	• Smaller • Can be reduced by minimized T_d	Larger
Medium D_L range 0.33<D_L<0.66	Power transfer interval (No circulating interval)		Power transfer interval (No circulating interval)	
High D_L range D_L>0.66	• Smaller • Can be reduced to zero when T_d is large enough	Larger	• Larger • Can be reduced by minimized T_d	• Smaller • Can be increased by minimized T_d

the two switching methods in this range are almost the same. Performance of two switching methods in this range are similar.

In the low D_L range, the power transfer and circulating current intervals are determined by value of D_L. The lower D_L is, the shorter the power transfer interval becomes, resulting in larger circulating current in both switching methods. The magnitude of circulating current I_{cir} of PPS is always smaller than that of DAPWM. Further, the magnitude of power transfer current I_{pow} of PPS is not affected by the dead time, whereas that of DAPWM is reduced by increased dead time T_d. Thus, it is concluded that PPS switching method is better to be used in the low D_L range. The calculated values of I_{pow}, I_{cir} of each switching method are detailed in the Table VII in the Appendix.

In the high D_L range, the larger D_L is, the shorter the power transfer interval becomes, resulting in larger circulating current in both PPS and DAPWM switching methods. When T_d increases, circulating current I_{cir} of PPS increases while that of DAPWM decreases. It is concluded that DAPWM switching method is better to be used in the high D_L range.

The detailed comparison of PPS and DAPWM switching methods in wide voltage range with the large dead time is summarized in Table II.

B. Power Flow Analysis

Assuming that the magnetizing current of the transformer is small and can be ignored, the relationship between primary and secondary winding currents of the transformer is given in (2) where $i_{pa,pb,pc}$ and $i_{a,b,c}$ are the primary and secondary winding currents, respectively. The power flow caculation is carried out based on the secondary winding current and power transfer interval, as shown in Fig. 2. Specifications of the bidirectional three-phase push–pull converter is given in Table V. The calculation results are listed in the Table VI. Fig. 3 shows the power

Authorized licensed use limited to: Seoul National Univ of Science & Tech (SNUT). Downloaded on November 06,2020 at 08:04:53 UTC from IEEE Xplore. Restrictions apply.

TABLE III
VOLTAGE RATIO V_L/V_{Cc} AND RANGE OF CONTROL VARIABLES DEPENDING ON d_l

Operation range of Duty cycle		V_L/V_{Cc}		Range of control variables	
		PPS	DAWPM	PPS	DAPWM
Reverse mode	D_L<0.33	$V_L/V_{Cc}=D_L$	$V_L/V_{Cc}=D_L$	$(D_L-1)<D_\varphi<-T_d/T_s$	$-(D_L/2-T_d/T_s)<\Delta D<-T_d/T_s$
	0.33<D_L<0.66	$V_L/V_{Cc}=D_L$	$V_L/V_{Cc}=D_L-T_d/T_s$	$D_\varphi<-T_d/T_s$	$-T_s/3<\Delta D<-T_d/T_s$
	D_L>0.66	$V_L/V_{Cc}=D_L$	$V_L/V_{Cc}=D_L-T_d/T_s$	$(D_L-1)<D_\varphi<-T_d/T_s$	$-T_s/3<\Delta D<-T_d/T_s$
Forward mode	D_L<0.33	$V_L/V_{Cc}=D_L+T_d/T_s$	$V_L/V_{Cc}=D_L$	$0<D_\varphi<D_L-T_d/T_s$	$T_d/T_s<\Delta D<T_s/3$
	0.33<D_L<0.66	$V_L/V_{Cc}=D_L+T_d/T_s$	$V_L/V_{Cc}=D_L+T_d/T_s$	$T_d/T_s<D_\varphi<T_s/3$	$T_d/T_s<\Delta D<T_s/3$
	D_L>0.66	$V_L/V_{Cc}=D_L+T_d/T_s$	$V_L/V_{Cc}=D_L+T_d/T_s$	$T_d/T_s<D_\varphi<1-(D_L-T_d/T_s)$	$T_d/T_s<\Delta D<(1-D_L)/2+T_d/T_s$

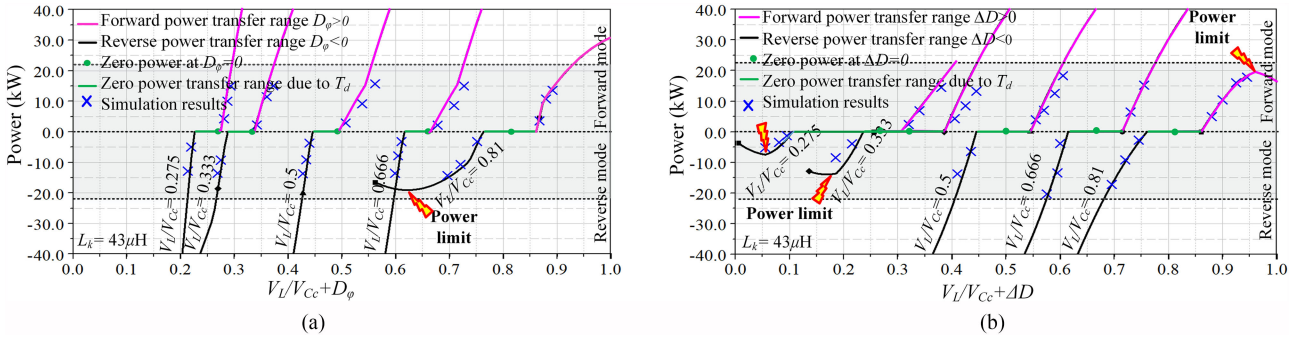

Fig. 3. Power flow under wide voltage range ($V_L = 220 \sim 650\ V, V_{Cc} = 800\ V, f_{sw} = 20$ kHz, $T_d = 2.5\ \mu s, L_k = 43\ \mu$H, $\mathrm{P_{max}} = 22$ kW). (a) PPS. (b) DAPWM.

TABLE IV
FEED FORWARD VALUE OF CLAMP VOLTAGE VCC CONTROL

		sign (I_L)	
		-1 (reverse mode)	1 (forward mode)
m	0 (PPS)	$D_{ff}=NV_L/V_H$	$D_{ff}=NV_L/V_H-T_d/T_s$
	1 (DAPWM)	$D_{ff}=NV_L/V_H-T_d/T_s$	$D_{ff}=NV_L/V_H+\Delta D_0$

TABLE V
SPECIFICATIONS OF THE THREE-PHASE CURRENT-FED PUSH–PULL BIDIRECTIONAL CONVERTER

Items	Symbol	Value
Low side voltage	V_L	220V~650V
High side voltage	V_H	745V
Maximum current	I_{Lmax}	55A (V_L= 220V~400V)
Maximum power	P_{max}	22kW(V_L= 400V~650V)
Switching frequency	f_s	20 kHz

TABLE VI
DESIGN PARAMETERS AND SELECTED DEVICES OF THE CONVERTER

Items	Values and Rating		Selected devices
Switches (S_{L1}-S_{L6}, S_{H1}-S_{H6})	V_{pk}	800 V	PMH75120S002
	I_{rms}	30 A	(R_{don}=0.09Ω , T_d= 2.5μs)
Clamp capacitor C_C	Value	90 μF	FE52N6L0306*B (3ea)
	V_{pk}	800 V	
Transformer turn ratio	N=N_s/N_p	13/14	EI-118 (2ea)
Leakage inductor L_k	Value	15 μH	-
Magnetizing inductor L_m	Value	2 mH	-
Filter inductor L_f	Value	300 μH	CH740125

flow analysis graphs of the converter with DAPWM and PPS switching methods

$$i_{pa,pb,pc} = i_{a,b,c} + \frac{1}{3} I_L. \tag{2}$$

Since the LVS voltage ranges from 220 to 650 V, the ratio of V_L/V_{Cc} largely varies from 0.275 to 0.81. Under varying condition of V_L, V_{Cc} is controlled by D_L so that V_{Cc} is fixed at 800 V (equal to V_H/N), and the transferred powers of PPS and DAPWM switching methods are calculated as function of D_φ and ΔD, and the results are shown in Fig. 3(a) and (b), respectively. The simulation results are in close agreement with the calculation results.

It is seen that both DAPWM and PPS switching methods with $L_k = 43\ \mu$H have a limitation of power transfer capability caused by narrow power transfer interval when $D_L < 0.33$ or $D_L > 0.66$. Power transfer capability of DAPWM is dramatically reduced in low D_L range due to small power transfer area and dominant circulating current area as analysis in Fig. 2. Reducing leakage inductance L_k increases the transfer power as shown in Fig. 4. In the high (>0.66) D_L range, the value of L_k has to be smaller than 34 and 35 μH for delivering the rated power of 22 kW with PPS and DAPWM, respectively. However, as L_k decreases the slew rate of transformer winding current increases, resulting in increased conduction losses. The detailed design of L_k is described in Section IV.

In general, between the forward and reverse power transfer ranges of the converter, there is a zero power transfer range caused by the dead time in which the transfer power is zero even

Authorized licensed use limited to: Seoul National Univ of Science & Tech (SNUT). Downloaded on November 06,2020 at 08:04:53 UTC from IEEE Xplore. Restrictions apply.

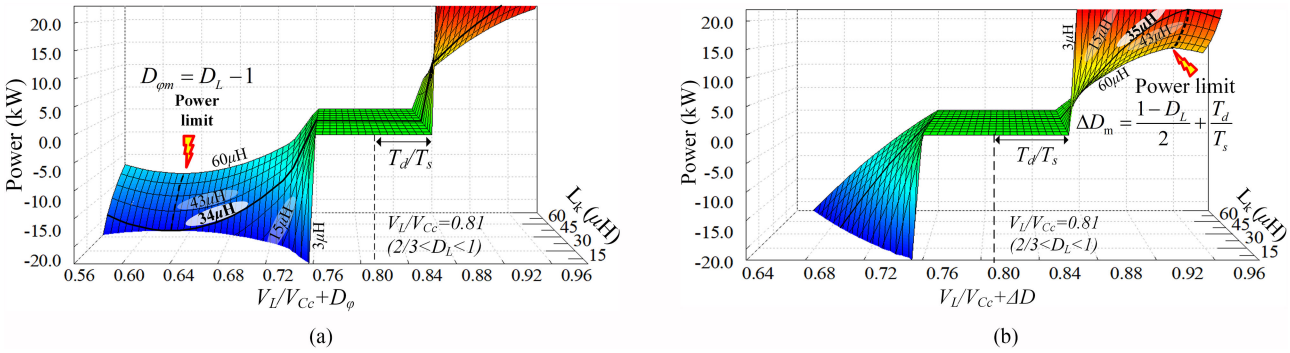

Fig. 4. Power flow with different leakage inductance L_k at $V_L/V_{Cc} = 0.81$. (a) PPS. (b) DAPWM.

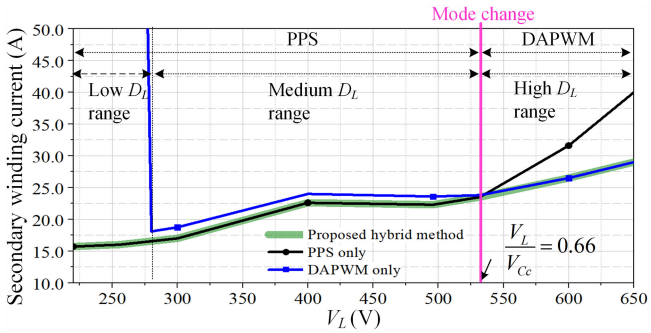

Fig. 5. RMS current of transformer secondary winding with PPS, DAPWM, and proposed hybrid control.

though the control variables varies. The power starts to increase when the control variables reach to a knee value, which causes a small delay in transient response of the system. This effect of zero power transfer range depending on the magnitude of dead time is shown to be trivial and can be eliminated by feed forward control when power is zero. The ranges of the control variables and voltage ratio V_L/V_{Cc} depending on D_L, T_d and power direction are expressed in Table III.

III. Proposed Hybrid PPS-DAPWM Switching Method

A. Principles of the Proposed Hybrid PPS-DAPWM Method

Fig. 5 shows the transformer secondary winding with PPS, DAPWM, and proposed hybrid method. The proposed hybrid method is aimed to reduce the circulating current and to increase the power transfer area in low (<0.33) and high (>0.66) D_L ranges. Thus, PPS is selected due to the advantage of larger power transfer area and smaller circulating current in the low and medium D_L range while DAPWM is selected due to the smaller circulating current in the high D_L range.

The mode change between PPS and DAPWM is defined at $V_L/V_{Cc} = 0.66$. The worst case in term of transformer winding current in high D_L range is determined at $V_L = 650\,\text{V}$. It is noted that the proposed hybrid method has smaller rms current by combining PPS and DAPWM switching methods.

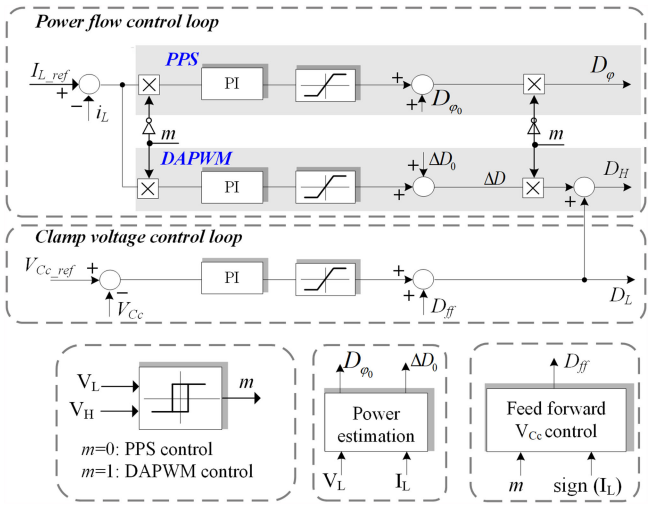

Fig. 6. Proposed hybrid PPS-DAPWM method with seamless control.

B. Seamless Mode Change of Hybrid PPS-DAPWM Method

During the mode change between PPS and DAPWM, the transients of the clamp voltage V_{Cc} and transfer power should be minimized. Fig. 6 shows control block diagram of the proposed hybrid PPS-DAPWM for seamless mode change, which includes feed forward V_{Cc} control block for regulating the clamp voltage and power estimation block for keeping the transferred power constant during the mode change.

The clamp voltage is controlled by D_L with the set point value of $V_{Cc\_ref} = V_H/N$. The reference value of transfer power is represented by I_{L_ref}. The detect mode signal m is used for selecting the switching mode: PPS or DAPWM. In order to prevent the unwanted rapid switching noise of V_{Cc} during measuring, controlling, and mode changing, the hysteresis band for V_{Cc} of 20 V is used.

The power estimation block observes the power from the measured value of LVS V_L and filter inductor current I_L and then gives the feed forward control variables $D_{\varphi 0}$ and ΔD_0 to the controller. Values of $D_{\varphi 0}$ and ΔD_0 depending on measured power can be determined by power flow formulas in Table VII.

Fig. 7 shows the simulation results of mode change. When $V_L/V_{Cc} < 0.66$, the PPS method is selected ($m = 0$,

Authorized licensed use limited to: Seoul National Univ of Science & Tech (SNUT). Downloaded on November 06,2020 at 08:04:53 UTC from IEEE Xplore. Restrictions apply.

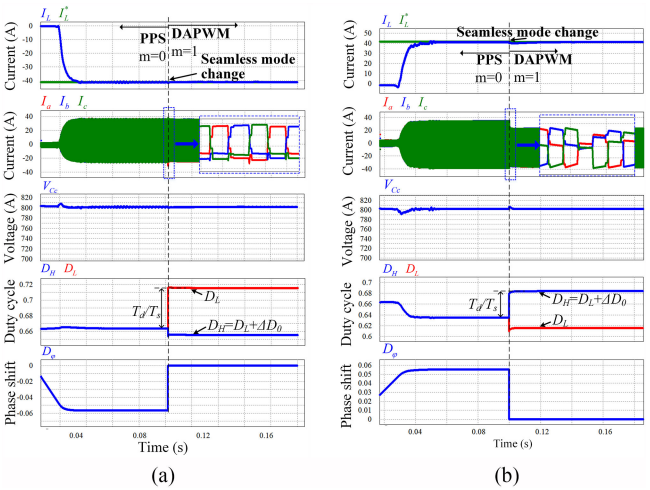

Fig. 7. Simulation waveforms of mode change from PPS to DAPWM. (a) Reverse mode. (b) Forward mode.

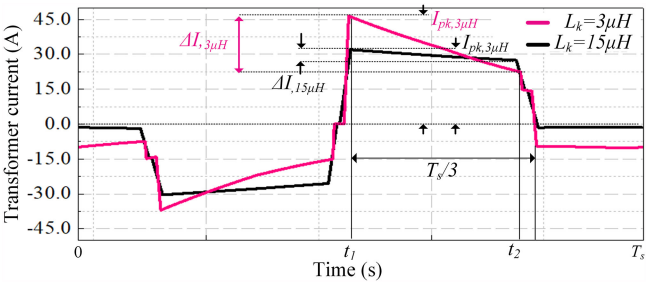

Fig. 8. Slew rate of transformer current with different L_k when $D_L = 0.66$.

$D_H = D_L$), the transferred power is controlled by D_φ. When m changes to 1, the feed forward control signal D_{ff} depending on different operation mode is determined for maintaining active clamp voltage V_{Cc} constant, as given in Table IV; the power estimation block gives $D_H = D_L + \Delta D_0$, which helps to keep filter inductor current I_L constant. It can be seen from the simulation results shown in Fig. 7(a) and (b) that V_{Cc} and I_L have trivial transient during the mode change.

IV. Design of Three-Phase Push–Pull DC–DC Converter

Table V summarizes the specifications of a 22-kW three-phase push–pull bidirectional dc–dc converter. The filter inductor and the active clamp capacitor are designed based on [13], and the designed values is listed in Table VI. This article focuses on design of the turn ratio of the transformer and the leakage inductance considering minimization of the transformer winding current and clamp voltage V_{Cc}.

From Figs. 4 and 5, it is seen that the highest of the transformer winding current and the limitation of power transfer capability occur at $V_L = 650$ V. The rated power of 22 kW can be achieved by reducing L_k and N. However, reducing N increases clamp voltage V_{Cc} resulting in increased voltage rating

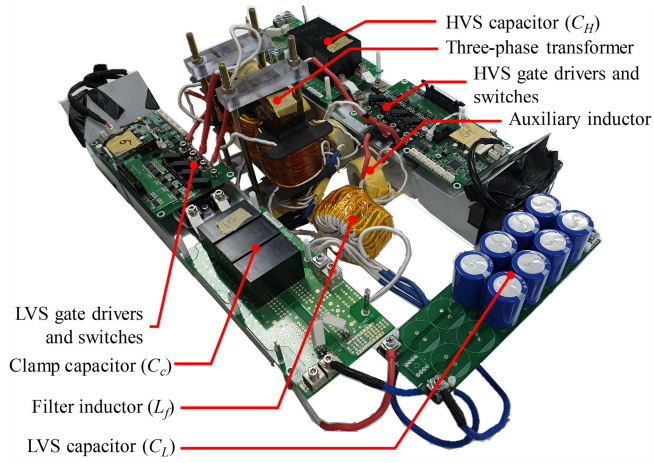

Fig. 9. Photograph of implemented 22 kW prototype of bidirectional three-phase push–pull converter.

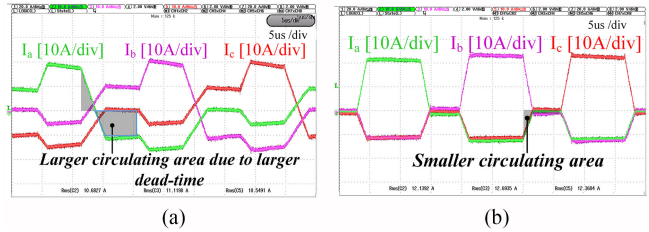

Fig. 10. Experimental results showing the effect of different switching methods on circulating current at $D_L = 0.81$ (high D_L range). (a) PPS. (b) DAPWM (proposed).

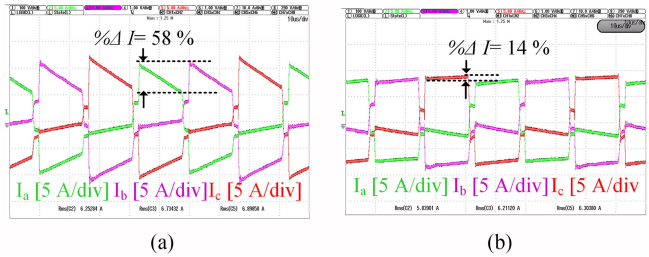

Fig. 11. Experimental results showing the effect of different L_k on the slew rate current at $P_o = 4$ kW. (a) $L_k = 3$ μH. (b) $L_k = 15$ μH (designed value).

of LVS switches. Also, reducing L_k increases the slew rate of the transformer winding current resulting in increased peak winding current, as shown in Fig. 8. The design procedure of L_k and N is detailed further.

A. Turn Ratio of Transformer N

The active clamp voltage is determined by

$$V_{Cc} = \frac{V_H}{N}. \tag{3}$$

In this design, the active clamp voltage V_{Cc} is limited to 800 V considering the voltage rating of the LVS switches, therefore N should be equal to or larger than 0.93. Since increasing the

Authorized licensed use limited to: Seoul National Univ of Science & Tech (SNUT). Downloaded on November 06,2020 at 08:04:53 UTC from IEEE Xplore. Restrictions apply.

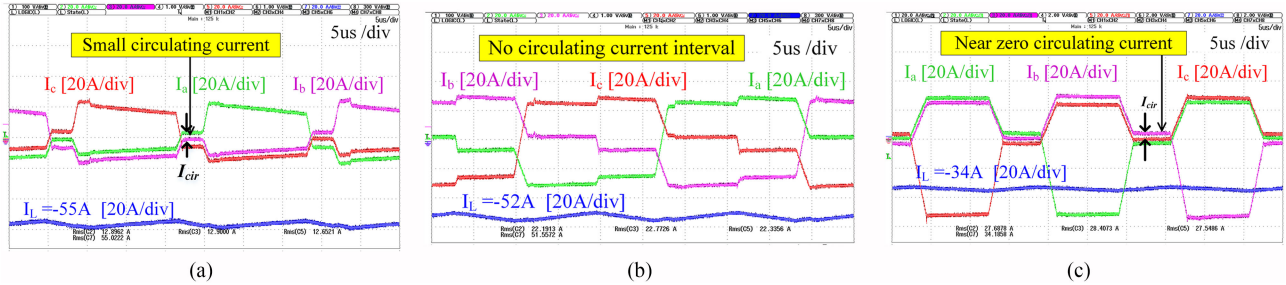

(a) (b) (c)

Fig. 12. Experimental waveforms of the filter inductor and secondary transformer current in the forward mode. (a) $V_L = 220\ V$, $D_L = 0.22$ (Low D_L), $P_o = 12$ kW with PPS method. (b) $V_L = 400\ V$, $D_L = 0.45$ (Medium D_L), $P_o = 21$ kW, with PPS method. (c) $V_L = 650\ V$, $D_L = 0.76$ (High D_L), $P_o = 22$ kW, with DAPWM method.

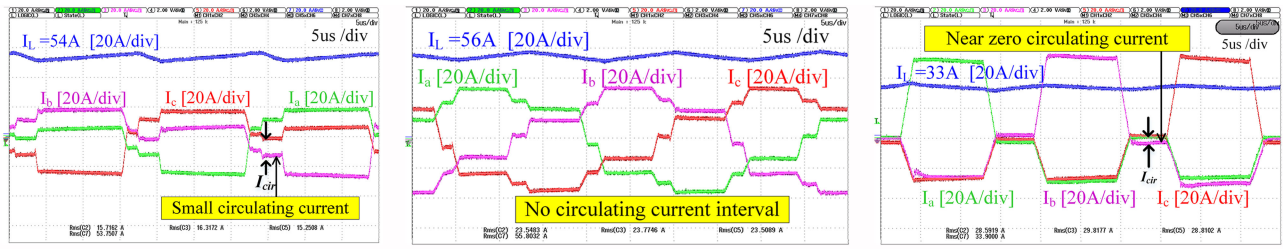

(a) (b) (c)

Fig. 13. Experimental waveforms of the filter inductor and secondary transformer current in the reverse mode (a) $V_L = 220$ V, $D_L = 0.27$ (Low D_L), $P_o = 11.8$ kW, with PPS method. (b) $V_L = 400$ V, $D_L = 0.50$ (Medium D_L), $P_o = 22.1$ kW, with PPS method. (c) $V_L = 650$ V, $D_L = 0.81$ (High D_L), $P_o = 22.5$ kW, with DAPWM method.

turn ratio increases the transformers winding current [25], N is selected to be 0.93.

B. Leakage Inductance L_k

With designed value of $N = 0.93$, the maximum value of L_k is calculated to be 35 μH for achieving the rate power of 22 kW at the worst case of $V_L = 650$ V.

Fig. 8 shows the secondary transformer current waveforms with different L_k. Although the active clamp control loop is aimed at making the transformer winding current as flat as possible during the interval of time $[t_1 - t_2]$ for minimizing rms current. However, the percentage change of transformer winding current $\%\Delta I$ also depends on leakage inductance and parasitic resistance as shown in the following [25]:

$$\%\Delta I = (1 - e^{-(r_{equ}/L_k)(t_2 - t_1)}) \times 100. \quad (7)$$

The equivalent resistance r_{equ} is experimentally estimated to be 0.15 Ω, includes ON-state resistance of switching devices and parasitic resistance. It can be seen from (7) that as L_k increases $\%\Delta I$ decreases. The minimum value of L_k is determined by limiting the slew rate of transformer winding current. The worst case slew rate of the transformer current occurs at $D_L = 0.66$, in which $[t_1 - t_2]$ is near $T_s/3$ as shown in Fig.8. $\%\Delta I$ is suggested to be less than or equal 15%. From (7), the minimum value of L_k is calculated to 15 μH as shown in Fig. 9, and the transformer winding current becomes nearly flat compared with $L_k = 3\ \mu H$. The range of the L_k can be obtained as follows:

$$15\mu\text{H} < L_k < 35\mu\text{H}. \quad (8)$$

Meanwhile, in general, increasing L_k causes higher transformer winding current. Thus, the value of L_k is selected to be 15 μH.

V. Experimental Results and Discussions

Fig. 9 shows the photograph of an implemented 22 kW prototype of the bidirectional three phase push–pull converter for battery changing and discharging application. The main specifications are summarized in Table V. Table VI shows design parameters and selected devices of the prototype.

As discussed in Fig. 5, DAPWM is chosen in the high ($D_L > 0.66$) D_L range, and PPS is chosen in the low ($D_L < 0.33$) and medium ($0.33 < D_L < 0.66$) D_L ranges for the proposed hybrid method. Fig. 10 shows the effect of different switching methods on circulating current at $V_L = 650$ V (in the high D_L range) where the DAPWM is shown to have much smaller circulating current compared to PPS.

Fig. 11 shows the effect of different values of L_k on the slew rate of transformer winding current. In the case of $L_k = 3\ \mu$H, $\%\Delta I$ is 58%, resulting in high rms current as shown in Fig. 11(a). With the designed value of $L_k = 15\ \mu$H, $\%\Delta I$ is reduced to 14%, as shown in Fig. 11(b). From Section IV, $\%\Delta I$ is calculated to 56.5% and 14.8% with $L_k = 3\ \mu$H and $L_k = 15\ \mu$H, respectively. The experimental results are in close agreement with the calculation results.

Figs. 12 and 13 show the experimental waveforms of the converter under wide voltage range of LVS ($0.222 < D_L$

Authorized licensed use limited to: Seoul National Univ of Science & Tech (SNUT). Downloaded on November 06,2020 at 08:04:53 UTC from IEEE Xplore. Restrictions apply.

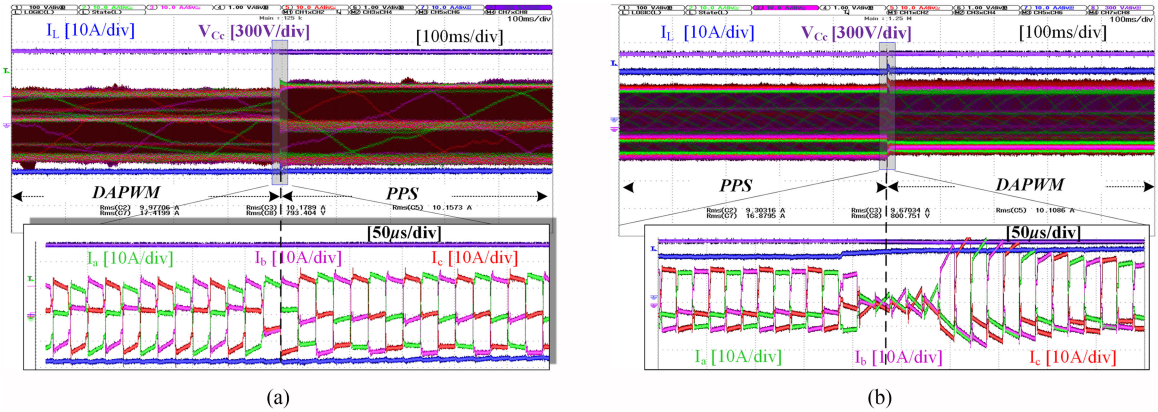

Fig. 14. Experimental results showing transient state during the mode change between PPS and DAPWM switching method ($P_o = 10$ kW, the mode change at $V_L = 530$ V, $V_H = 745$ V). (a) From DAPWM to PPS in the forward power flow. (b) From PPS to DAPWM in reverse power flow.

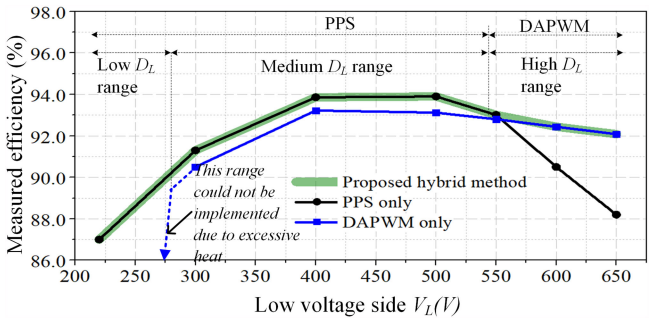

Fig. 15. Measured efficiencies of the converter with PPS, DAPWM and proposed hybrid switching method at $I_L = 22$ A (V_L<400 V), $I_L = 10$ kW/V_L (V_L>400 V).

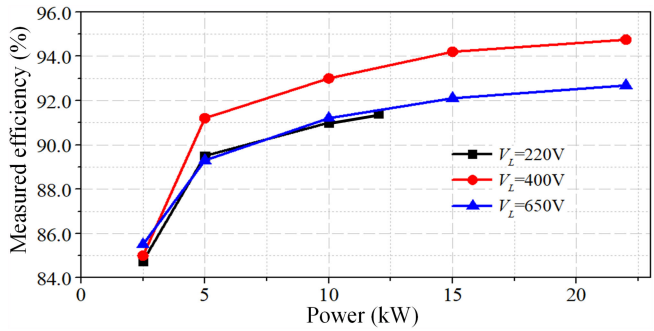

Fig. 16. Measured efficiency as a function of the output power, $I_{L\_max} = 55$ A ($V_L < 400$ V).

< 0.81) in the forward and reverse modes, respectively. When $V_L = 220$ V (in the low D_L range), as shown in Figs. 12(a) and 13(a), the circulating current is small. At $V_L = 400$ V (in the medium D_L range), as shown in Figs. 12(b) and 13(b), the converter operates without circulating current interval. When $V_L = 650$ V, it is noted from Figs. 12(c) and 13(c) that the rated power of 22 kW in both power flows was achieved with near zero circulating current.

In the battery charging and discharging application, the LVS voltage V_L is slowly reduced or increased, when V_L reaches 530 V ($V_L/V_{Cc} = 0.66$), the mode change between PPS and DAPWM occurs. Fig. 14 shows the experimental results of transient state during the mode change in both power flows. It is noted from Fig. 14(a) that the clamp voltage V_{Cc}, filter inductor current, and three-phase transformer currents have little transient during the mode change from DAPWM to PPS. Fig. 14(b) shows small overshoots of currents and voltage during several switching cycles from PPS to DAPWM, which is acceptable for normal operation of the transformer and switching devices.

Figs. 15 and 16 show the efficiency curves of the converter measured by YOKOGAWA WT3000. Three switching methods of the proposed hybrid, PPS only, and DAPWM only have been implemented with the prototype.

In Fig.15, in the low D_L range, DAPWM method could not be properly implemented due to excessive heat of switching devices caused by dominant circulating current and small power transfer area, as discussed in Section II. The PPS method has lower efficiency than the DAPWM method in the high D_L range due to high circulating current, as shown in Fig. 15. It is concluded that the proposed hybrid switching method significantly improves the efficiencies especially in low and high D_L ranges compared to PPS and DAPWM only methods.

Fig. 16 shows the measured efficiency of the converter as a function of the output power with proposed hybrid switching.

VI. Conclusion

This article proposed a hybrid switching method for efficiency improvement of the bidirectional three-phase push–pull converter with *wide* voltage range. The problems related to *wide* voltage range operation such as limitation on power transfer capability, effect of slew rate of transformer winding current, and dead-time effect on circulating current were analyzed in detail. Through the analysis, an optimized design of L_k value along with transformer turn ratio was also proposed to minimize the rms current of transformer winding, limit the slew rate of transformer winding current to 15%, and have the capability of transferring the desired power. Further, two switching methods of PPS and DAPWM were compared in terms of dead-time effect on circulating current and power transfer area. The hybrid

Authorized licensed use limited to: Seoul National Univ of Science & Tech (SNUT). Downloaded on November 06,2020 at 08:04:53 UTC from IEEE Xplore. Restrictions apply.

TABLE VII
TRANSFORMER SECONDARY CURRENT AND POWER TRANSFER EQUATION OF PPS AND DAPWM

		$D_L < 0.33$	$0.33 < D_L < 0.66$	$D_L > 0.66$
DAPWM	Reverse mode	$I_{cir} = \begin{cases} \frac{1}{3}\frac{V_H}{NL_k}(2\Delta DT_s + 2T_d) & if\ (\Delta DT_s > -3T_d) \\ \frac{1}{3}\frac{V_H}{NL_k}(\Delta DT_s - T_d) & if\ (\Delta DT_s \le -3T_d) \end{cases}$ $I_{pow} = I_{cir} + \frac{2}{3}\frac{V_H}{NL_k}T_d$ $P = \frac{3}{T_s}\frac{V_H I_{pow}}{N}((D_L + \Delta D)T_s - T_d)$	$I_{pow} = \frac{2}{3}\frac{V_H}{NL_k}(\Delta DT_s + T_d)$ $P = \frac{3}{T_s}\frac{V_H I_{pow}}{N}(\frac{T_s}{3} + \frac{2\Delta DT_s}{3})$	$I_{cir} = \begin{cases} 0 & if\ (\Delta DT_s \ge -2T_d) \\ \frac{2}{3}\frac{V_H}{L_k N}(\Delta DT_s + 2T_d) & if\ (\Delta DT_s < -2T_d) \end{cases}$ $I_{pow} = \frac{2}{3}\frac{V_H}{L_k N}(\Delta DT_s + 2T_d)$ $P = \frac{3}{T_s}\frac{V_H I_{pow}}{N}((1 - D_H + \frac{\Delta D}{2})T_s - \frac{T_d}{2})$
	Forward mode	$I_{cir} = \frac{1}{3}\frac{V_H}{L_k N}\Delta DT_s$ $I_{pow} = I_{cir} - \frac{2}{3}\frac{V_H}{L_k N}T_d$ $P = \frac{3}{T_s}\frac{V_H}{N}(I_{pow}(\frac{\Delta DT_s}{2} + D_L T_s) + \frac{I_{cir}}{2}(-\Delta DT_s + 2T_d))$	$I_{pow-1} = \frac{1}{3}\frac{V_H}{NL_k}\frac{4(\Delta DT_s - T_d)}{3}$ $I_{pow-2} = \frac{1}{3}\frac{V_H}{NL_k}\frac{2(\Delta DT_s - T_d)}{3}$ $P = \frac{V_H}{T_s N}(I_{pow-1}(T_s - \Delta DT_s - 2T_d) + I_{pow-2}(4T_d - \Delta DT_s))$	$I_{cir} = \begin{cases} 0 & if\ (\Delta DT_s < 2T_d) \\ \frac{2}{3}\frac{V_H}{L_k N}(\Delta DT_s - 2T_d) & if\ (\Delta DT_s \ge 2T_d) \end{cases}$ $I_{pow} = \frac{2}{3}\frac{V_H}{L_k N}(\Delta DT_s - T_d)$ $P = \begin{cases} \frac{3}{T_s}\frac{V_H}{N}(I_{pow}(1 - D_H)T_s + \frac{I_{pow} + I_{cir}}{2}(\Delta DT_s - T_d) & if\ (\Delta DT_s < 2T_d) \\ \frac{3}{T_s}\frac{V_H}{N}(I_{pow}(1 - D_H)T_s + \frac{I_{pow} + I_{cir}}{2}T_d & if\ (\Delta DT_s \ge 2T_d) \end{cases}$
PPS	Reverse mode	$I_{cir} = \begin{cases} -\frac{1}{3}\frac{V_H}{NL_k}T_d & if\ (D_\varphi T_s > -\frac{T_d}{2}) \\ \frac{2}{3}\frac{V_H}{NL_k}(D_\varphi T_s + T_d) & if\ (D_\varphi T_s \le -\frac{T_d}{2}) \end{cases}$ $I_{pow} = I_{cir} + \frac{2}{3}\frac{V_H}{N}(D_\varphi T_s + T_d)$ $P = \frac{3V_H}{N}(I_{pow}(D_L + D_\varphi) - \frac{(I_{pow} + I_{cir})}{2}(D_\varphi + \frac{T_d}{T_s}))$	$I_{pow-1} = \begin{cases} \frac{2}{3}\frac{V_H}{L_k N}(\frac{1}{2}D_\varphi T_s) & if\ (D_\varphi T_s < -2T_d) \\ \frac{2}{3}\frac{V_H}{L_k N}(D_\varphi T_s + T_d) & if\ (D_\varphi T_s \ge -2T_d) \end{cases}$ $I_{pow-2} = \begin{cases} \frac{2}{3}\frac{V_H}{L_k N}(D_\varphi T_s) & if\ (D_\varphi T_s < -2T_d) \\ \frac{4}{3}\frac{V_H}{L_k N}(D_\varphi T_s + T_d) & if\ (D_\varphi T_s \ge -2T_d) \end{cases}$ $P = \frac{3}{T_s}\frac{V_H}{N}(I_{pow-2}(\frac{T_s}{3} + \frac{D_\varphi}{2}\mathrm{T_s})) - \frac{I_{pow-1}}{2}(D_\varphi \mathrm{T_s})$	$I_{cir} = \begin{cases} -\frac{1}{3}\frac{V_H}{L_k N}T_d & if\ (D_\varphi T_s > \frac{-\mathrm{T_d}}{2}) \\ \frac{2}{3}\frac{V_H}{L_k N}(D_\varphi T_s + T_d) & if\ (D_\varphi T_s \le \frac{-\mathrm{T_d}}{2}) \end{cases}$ $I_{pow} = I_{cir} + \frac{2}{3}\frac{V_H}{L_k N}(D_\varphi T_s + T_d)$ $P = \frac{3V_H}{N}(I_{pow}(1 - D_L + D_\varphi) - \frac{I_{pow} + I_{cir}}{2}(D_\varphi + \frac{T_d}{T_s}))$
	Forward mode	$I_{pow} = \frac{2}{3}\frac{V_H}{L_k N}(D_\varphi T_s + T_d)$ $P = \frac{3}{T_s}V_H(I_{pow}(D_L T_s - \frac{D_\varphi}{2}\mathrm{T_s} + T_d))$	$I_{pow} = \begin{cases} \frac{1}{3}\frac{V_H}{L_k N}(2D_\varphi T_s - T_d) & if\ (D_\varphi T_s > T_d) \\ \frac{1}{3}\frac{V_H}{L_k N}(D_\varphi T_s) & if\ (D_\varphi T_s < T_d) \end{cases}$ $P = 3\frac{V_H}{N}I_{pow}(\frac{1}{3} - \frac{1}{2}D_\varphi)$	$I_{cir} = \begin{cases} \frac{1}{3}\frac{V_H}{L_k N}(T_d) & if\ (D_\varphi T_s > \frac{3T_d}{2}) \\ \frac{2}{3}\frac{V_H}{L_k N}(D_\varphi T_s - T_d) & if\ (D_\varphi T \le \frac{3T_d}{2}) \end{cases}$ $I_{pow} = I_{cir} + \frac{2}{3}\frac{V_H}{L_k N}(D_\varphi T_s - T_d)$ $P = \frac{3V_H}{N}(-I_{pow}(1 - D_L - D_\varphi) - \frac{I_{cir} - I_{pow}}{2}D_\varphi)$

PPS-DAPWM method was proposed for minimizing circulating current, in which the PPS is chosen in the low ($D_L < 0.33$) and medium ($0.333 < D_L < 0.66$) D_L ranges, and DAPWM is chosen in the high ($D_L > 0.66$) D_L range. A seamless mode change method between PPS and DAPWM was also proposed for minimizing the transient state.

Experimental results from a 22-kW prototype were provided to validate the proposed concept. The proposed hybrid switching method significantly improved the efficiencies especially in low and high D_L ranges compared to PPS and DAPWM only methods.

APPENDIX

The circulating current and power equations of different working modes and duty cycle ranges are established in the Table VII, which are carried out based on the secondary winding current and the power transfer interval.

REFERENCES

[1] R. W. A. A. De Doncker, D. M. Divan, and M. H. Kheraluwala, "A three-phase soft-switched high-power-density DC/DC converter for high-power applications," *IEEE Trans. Ind. Appl.*, vol. 27, no. 1, pp. 63–73, Jan./Feb. 1991.

[2] N. H. Baars, J. Everts, C. G. E. Wijnands, and E. A. Lomonova, "Performance evaluation of a three-phase dual active bridge DC– converter with different transformer winding configurations," *IEEE Trans. Power Electron.*, vol. 31, no. 10, pp. 6814–6823, Oct. 2016.

[3] P. Xuewei and A. K. Rathore, "Naturally clamped soft-switching current-fed three-phase bidirectional DC/DC converter," *IEEE Trans. Ind. Electron.*, vol. 62, no. 5, pp. 3316–3324, May 2015.

[4] J. Hu, P. Joebges, G. C. Pasupuleti, N. R. Averous, and R. W. De Doncker, "A maximum-output-power-point-tracking-controlled dual-active bridge converter for photovoltaic energy integration into MVDC grids," *IEEE Trans. Energy Convers.*, vol. 34, no. 1, pp. 170–180, Mar. 2019.

Authorized licensed use limited to: Seoul National Univ of Science & Tech (SNUT). Downloaded on November 06,2020 at 08:04:53 UTC from IEEE Xplore. Restrictions apply.

[5] D. Wang, B. Nahid-Mobarakeh, and A. Emadi, "Second harmonic current reduction for a battery-driven grid interface with three-phase dual active bridge DC– converter," *IEEE Trans. Ind. Electron.*, vol. 66, no. 11, pp. 9056–9064, Nov. 2019.
[6] H. van Hoek, M. Neubert, and R. W. De Doncker, "Enhanced modulation strategy for a three-phase dual active bridge—Boosting efficiency of an electric vehicle converter," *IEEE Trans. Power Electron.*, vol. 28, no. 12, pp. 5499–5507, Dec. 2013.
[7] S. P. Engel, M. Stieneker, N. Soltau, S. Rabiee, H. Stagge, and R. W. De Doncker, "Comparison of the modular multilevel DC converter and the dual-active bridge converter for power conversion in HVDC and MVDC grids," *IEEE Trans. Power Electron.*, vol. 30, no. 1, pp. 124–137, Jan. 2015.
[8] N. H. Baars, J. Everts, H. Huisman, J. L. Duarte, and E. A. Lomonova, "A 80-kW isolated DC–DC converter for railway applications," *IEEE Trans. Power Electron.*, vol. 30, no. 12, pp. 6639–6647, Dec. 2015.
[9] F. Xue, R. Yu, and A. Q. Huang, "A 98.3% efficient GaN isolated bidirectional DC–DC converter for DC microgrid energy storage system applications," *IEEE Trans. Ind. Electron.*, vol. 64, no. 11, pp. 9094–9103, Nov. 2017.
[10] H. Cha, J. Choi, and P. N. Enjeti, "A three-phase current-fed DC/DC converter with active clamp for low-DC renewable energy sources," *IEEE Trans. Power Electron.*, vol. 23, no. 6, pp. 2784–2793, Nov. 2008.
[11] J. Choi, H. Cha, and B. Han, "A three-phase interleaved DC–DC converter with active clamp for fuel cells," *IEEE Trans. Power Electron.*, vol. 25, no. 8, pp. 2115–2123, Aug. 2010.
[12] Z. Wang and H. Li, "A soft switching three-phase current-fed bidirectional DC-DC converter with high efficiency over a wide input voltage range," *IEEE Trans. Power Electron.*, vol. 27, no. 2, pp. 669–684, Feb. 2012.
[13] M. Kwon, J. Park, and S. Choi, "A bidirectional three-phase push–pull converter with dual asymmetrical PWM method," *IEEE Trans. Power Electron.*, vol. 31, no. 3, pp. 1887–1895, Mar. 2016.
[14] Z. Wang and H. Li, "An integrated three-port bidirectional DC–DC converter for PV application on a DC distribution system," *IEEE Trans. Power Electron.*, vol. 28, no. 10, pp. 4612–4624, Oct. 2013.
[15] K. R. Sree and A. K. Rathore, "Impulse commutated high-frequency soft-switching modular current-fed three-phase DC/DC converter for fuel cell applications," *IEEE Trans. Ind. Electron.*, vol. 64, no. 8, pp. 6618–6627, Aug. 2017.
[16] R. L. Andersen and I. Barbi, "A ZVS-PWM three-phase current-fed push–pull DC–DC converter," *IEEE Trans. Ind. Electron.*, vol. 60, no. 3, pp. 838–847, Mar. 2013.
[17] S. Bal, A. K. Rathore, and D. Srinivasan, "Naturally clamped snubberless soft-switching bidirectional current-fed three-phase push–pull DC/DC converter for DC microgrid application," *IEEE Trans. Ind. Appl.*, vol. 52, no. 2, pp. 1577–1587, Mar./Apr. 2016.
[18] S. Lee, J. Park, and S. Choi, "A three-phase current-fed push–pull DC–DC converter with active clamp for fuel cell applications," *IEEE Trans. Power Electron.*, vol. 26, no. 8, pp. 2266–2277, Aug. 2011.
[19] K. R. Sree and A. K. Rathore, "Analysis and design of impulse-commutated zero-current-switching single-inductor current-fed three-phase push–pull converter," *IEEE Trans. Ind. Appl.*, vol. 53, no. 2, pp. 1517–1526, Mar./Apr. 2017.
[20] R. L. Andersen and I. Barbi, "A three-phase current-fed push–pull DC–DC converter," *IEEE Trans. Power Electron.*, vol. 24, no. 2, pp. 358–368, Feb. 2009.
[21] H. R. E. Larico and I. Barbi, "Three-phase push–pull DC–DC converter: analysis, design, and experimentation," *IEEE Trans. Ind. Electron.*, vol. 59, no. 12, pp. 4629–4636, Dec. 2012.
[22] A. I. Pressman, K. Billings, and T. Morey, "Current-mode and current-fed topologies," in *Switching Power Supply Design*, 3rd ed. New York, NY, USA: McGraw-Hill, 2007, pp. 161–227.
[23] D. Sha, Q. Lin, F. You, X. Wang, and G. Xu, "A ZVS bidirectional three-level DC–DC converter with direct current slew rate control of leakage inductance current," *IEEE Trans. Power Electron.*, vol. 52, no. 3, pp. 2368–2377, May 2016.
[24] L. Xu, D. Sha, and H. Chen, "A ZVS bidirectional three-level DC–DC converter with direct current slew rate control of leakage inductance," in *Proc. IEEE Energy Convers. Congr. Expo.*, Sep. 2014, pp. 4410–4415.
[25] T. Le, H. Jeong, S. Kim, and S. Choi, "Analysis, design and implementation of a bidirectional three-phase push-pull converter for wide voltage range application," in *Proc. 10th Int. Conf. Power Electron. ECCE Asia (ICPE 2019 - ECCE Asia)*, Busan, South Korea, 2019, pp. 2880–2885.
[26] R. B. Sepe and J. H. Lang, "Inverter nonlinearities and discrete-time vector current control," *IEEE Trans. Ind. Appl.*, vol. 30, no. 1, pp. 62–70, Jan./Feb. 1994.
[27] X. Ding *et al.*, "Analytical and experimental evaluation of SiC-inverter nonlinearities for traction drives used in electric vehicles," *IEEE Trans. Power Electron.*, vol. 67, no. 1, pp. 146–159, Jan. 2018.
[28] D. Wang, F. Peng, J. Ye, Y. Yang, and A. Emadi, "Dead-time effect analysis of a three-phase dual-active bridge DC/DC converter," *IET Power Electron.*, vol. 11, no. 6, pp. 984–994, 2018.
[29] D. Costinett, D. Maksimovic, and R. Zane "Design and control for high efficiency in high step-down dual active bridge converters operating at high switching frequency," *IEEE Trans. Power Electron.*, vol. 28, no. 8, pp. 3931–3940, Aug. 2013.
[30] D. Sha, X. Wang, K. Liu, and C. Chen, "A current-fed dual-active-bridge DC–DC converter using extended duty cycle control and magnetic-integrated inductors with optimized voltage mismatching control," *IEEE Trans. Power Electron.*, vol. 34, no. 1, pp. 462–473, Jan. 2019.

Tat-Thang Le was born in Haiphong, Vietnam. He received the B.E. degree from the Department of Electrical Engineering, Hanoi University of Science and Technology, Hanoi, Vietnam and the M.S. degree from the Department of Electrical Engineering, Changwon National Univeristy, South Korea, all in electrical engineering, in 2015 and 2017, respectively. He is currently working toward the Ph.D. degree with the Department of Electrical and Information Engineering, Seoul National University of Science and Technology, Seoul, South Korea.

His research interests include bidirectional dc–dc converter and high power dc–dc converter and power conversion technologies for fast charger system, renewable energy system, and electrical vehicles.

Hyeonju Jeong was born in South Korea, in 1989. He received the B.S. degree from the Department of Electronics and Electrical Engineering, Dankook University and the MS degree from the Department of Electrical and Information engineering, Seoul National University of Science and Technology (Seoul Tech), all in electrical engineering, in 2014 and 2016, respectively. He is currently working toward the Ph.D. degree in electrical and information engineering at Seoul Tech, Seoul, South Korea.

His research interests include bidirectional dc–dc converter and resonant converter for electric vehicles and renewable energy systems.

Sewan Choi (Fellow, IEEE) received the M.S. and Ph.D. degrees in electrical engineering from Texas A&M University, College Station, TX, USA, in 1992 and 1995, respectively.

From 1985 to 1990, he was a Research Engineer with Daewoo Heavy Industries. From 1996 to 1997, he was a Principal Research Engineer with Samsung Electro-Mechanics Company, Seoul, South Korea. In 1997, he joined the Department of Electrical and Information Engineering, Seoul National University of Science and Technology (Seoul Tech), Seoul, South Korea, where he is currently a Professor. From 2017 to 2018, he was the Vice President of Korean Institute of Power Electronics, Seoul, where he is currently the Senior Vice President. His research interests include power conversion technologies for renewable energy systems and dc–dc converters and battery chargers for electric vehicles.

Dr. Choi was a Technical Programme Comittee Chair of International Conference on Power Electronics - IEEE Energy Conversion Congress & EXPO Asia (ICPE2019-IEEE ECCE Asia) held in Busan, Korea. He is currently an Associate Editor for the IEEE TRANSACTIONS ON POWER ELECTRONICS and IEEE JOURNAL ON EMERGING AND SELECTED TOPIC IN POWER ELECTRONICS.

Authorized licensed use limited to: Seoul National Univ of Science & Tech (SNUT). Downloaded on November 06,2020 at 08:04:53 UTC from IEEE Xplore. Restrictions apply.